Microfluid Nanofluid
DOI 10.1007/s10404-010-0656-6

RESEARCH PAPER

Optimizing mixing in channel flows: kinematic aspects associated with secondary flows in the cross-section

Kevin L. McIlhany · Stephen Wiggins

Received: 30 March 2010 / Accepted: 20 May 2010
© US Government 2010

Abstract We consider an Eulerian predictor of optimal mixing appropriate for steady, three-dimensional channel flow of the type that is commonly used in a variety of microfluidic mixing applications. This *Eulerian indicator* is applied to a kinematic model of the channel flow that allows one to control the flow structure of the secondary flows and the number of distinct secondary flows. The cases of two and three distinct secondary flows are considered and the Eulerian indicator predicts the optimal flow structure in the two secondary flow case and in the three secondary flow case that result in the best mixing. Moreover, it is shown that the case of three secondary flows mixes "optimally" (i.e., faster and more completely) than the case of two secondary flows. An explanation of this difference is given in terms of the Eulerian flow structure.

Keywords Mixing · Chaotic advection · Channel flow · Kinematic model · Secondary flow · Eulerian indicators

1 Introduction

In this work, we are concerned with characterizing the kinematic features leading to "good mixing" in terms of Eulerian quantities. In this paper we are considering mixing due to advection alone, i.e., we are *not* considering the effect of molecular diffusion. Characterizing mixing in terms of Eulerian quantities may seem like an area where it is not possible to achieve much, practically, since mixing is fundamentally a Lagrangian process. It is concerned with the relative displacement, over time, of fluid particles with respect to their initial locations. This implies that, at a given time, a knowledge of the history of the relative displacements of fluid particles is required that is *not* evident from the fluid dynamical equations of motion whose solution is the velocity field that generates the flow. Indeed, the Lagrangian complexity generated by chaotic advection was not "seen" at all solely through examining properties of the velocity field. It was not until the 1980s, when it became widely possible to simulate mixing processes on computers that the full Lagrangian nature of mixing became widely appreciated. The dynamical systems point of view played a significant role in our understanding of mixing by introducing notions such as Poincaré maps, islands of unmixed fluids ("KAM tori"), deterministic chaos, and finite-time Lyapunov exponents (FTLEs), which provided new insights alongside with traditional measures of the quality of mixing such as the decay of variance of concentration. We refer to these quantities that describe certain Lagrangian aspects of the flow as *Lagrangian diagnostics*, and make the important observation that, with respect to mixing, they are *retrodictive*, rather than predictive, i.e., one must simulate the mixing process in order to compute these quantities. This is a significant observation with respect to the issue of the *design of optimal mixers* since, ideally, one would like to choose the geometrical parameters, boundary conditions, method for driving the flow, and other parameters resulting in the design of a mixer that produces a flow that mixes optimally (where "optimal" needs a careful consideration according to the requirements). This seems like too much to ask, however, it is not unreasonable, based on experience, to imagine that one

K. L. McIlhany (✉)
Physics Department, U. S. Naval Academy, Stop 9c,
572c Holloway RD, Annapolis, MD 21402-5002, USA
e-mail: mcilhany@usna.edu

S. Wiggins
School of Mathematics, University of Bristol, University Walk,
Bristol BS8 1TW, UK
e-mail: s.wiggins@bristol.ac.uk

Published online: 06 August 2010

could design a mixer that would create a velocity field having certain kinematic features, but it is not at all clear which kinematic features of a velocity field would result in optimal mixing.

With the insight of chaotic advection, coupled with considerable intuition derived from experiments, several authors have proposed Eulerian quantities that characterize the promotion of "good mixing." In particular, in Ottino (1990) the observation was made that "streamline crossing" is responsible for chaotic fluid particle trajectories. The phrase "streamline crossing" requires explanation. The two most common meanings are:

1. when the instantaneous streamline patterns at two different times are superimposed, they exhibit "crossing,"
2. for a steady, spatially periodic three-dimensional flow if the secondary flows in the cross-section at the beginning of a period and at half of a period are superimposed, then they exhibit "crossing."

In Sturman and Wiggins (2009) *Eulerian indicators* were introduced that quantified the notion of "streamline crossing" and "transversely oriented shears" for time-periodic, or steady spatially periodic flows, i.e., flows having two distinct "patterns" where streamline crossing and transversely oriented shears could be measured and quantified. It was shown that these Eulerian indicators were accurate *predictors* of optimal mixing (in the sense of "complete mixing" or the lack of unmixed regions) as a function of the parameters associated with the velocity field.

In this article, we generalize the Eulerian indicator that quantifies streamline crossing to the case of more than two distinct flow patterns. A particular application motivating this generalization concerns generating and optimizing mixing of two adjacent streams of different fluids flowing through a channel, or duct, which is a fundamental problem in many applications of microfluidic and nanofluidic flows. At these length scales, turbulence is not available to promote mixing and the problem, eloquently described by Knight (2002) is " like trying to stir molasses into honey, and two liquids traveling side-by-side through a narrow channel only become fully mixed after many centimetres." This article is concerned with understanding the kinematic conditions leading to "optimal" mixing in such flows and the development of *predictive* tools that will enable one to determine when such conditions arise in specific flows.

In order to fix a precise description of the situations that we are considering, let z denote the axial coordinate of the channel and let x and y denote the transverse, or cross-sectional, coordinates. We assume that the two streams of fluid move according to the same *steady*, three-dimensional velocity field. If there is no component of velocity in the x or y direction then there is no mixing of the streams, except by molecular diffusion. Similarly, if the x and y components of velocity are nonzero, but are independent of the axial coordinate z, then there is very poor mixing of the two streams. However, if the x and y components of velocity depend upon the axial coordinate, then as the two streams move down the channel they can be stretched and folded amongst each other, which is the hallmark of chaotic mixing. In summary, as the fluid moves down the channel it must experience a different cross-sectional velocity at different locations along the channel axis in order to "mix well."

Over the past 10 years, numerous groups have developed a variety of schemes for generating secondary flows that promote mixing. Perhaps the most well-known scheme is the staggered herringbone mixer (SHM) described in Stroock et al. (2002). For this mixer, the flow is driven by a pressure gradient and transverse components of velocity are created by a spatially periodic pattern of two types of herringbone-shaped grooves in the bottom of the channel. This raised the obvious question, specific to this type of channel micromixer, as to whether or not the geometry of the grooves is such that it generates "optimal" mixing. This question has been addressed using computational fluid dynamics techniques by Aubin et al. (2005) and Yang et al. (2005). Models of the SHM based on lid driven cavity flows have been considered by Stroock and McGraw (2004), Chen and Stremler (2009), and Song et al. (2008), where the walls, with the imposition of no-slip boundary conditions, are moved in a way that simulated the secondary flows generated by the herringbone patterns and the axial motion of the fluid is governed by an imposed pressure driven Poiseuille flow.

The common feature in this work is that the flow pattern of the secondary flow in the cross-section contains two recirculation gyres divided by a separatrix extending from the top to the bottom of the channel, where the location of the separatrix is fixed by the particular manner in which the secondary flow is created; either by the location of the "elbow" in the grooves on the bottom of the channel or in the manner in which the boundary of the cavity is moved. Figures 1 and 2 illustrate the streamlines of this flow. Moreover, the flows are spatially periodic in the sense that two distinct secondary flow patterns are experienced by the fluid as it moves down the channel. In the SHM mixer, as well as in the associated studies and models described above, the separatrices in the two secondary flows are symmetrically located about the vertical line in the middle of the channel. A question that arises is whether or not more general types of secondary flows will lead to "better" mixing, i.e., more complete mixing in a shorter length of channel? This is a difficult question to answer following the approaches described in the works above since fabricating micromixers and carrying out measurements on their mixing characteristics can be expensive and time consuming. Simulating micromixers

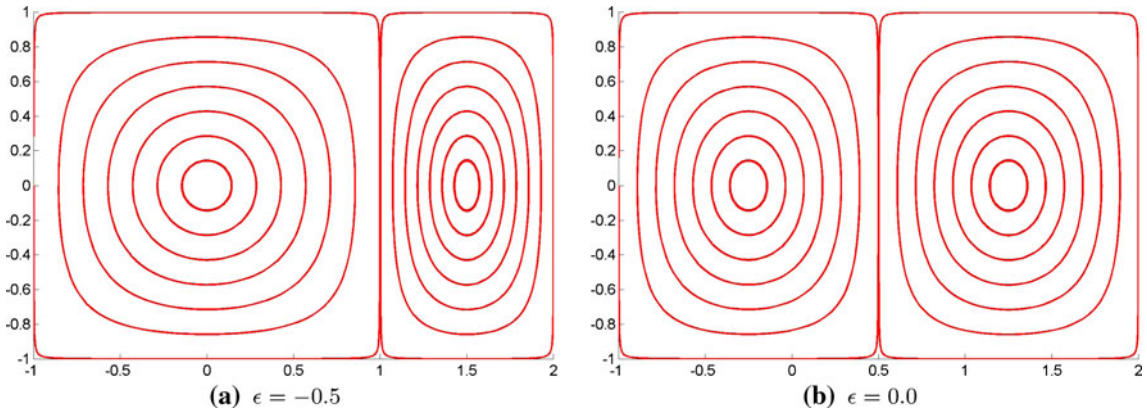

Fig. 1 Streamline patterns for two different values of ε. **a** corresponds to $b_1 = 0.0$, $c_1 = 1.0$, $b_2 = 1.5$, $c_2 = 0.5$, $\varepsilon = -0.5$ and **b** corresponds to $b_1 = -0.25$, $c_1 = 0.75$, $b_2 = 1.25$, $c_2 = 0.75$, $\varepsilon = 0.0$

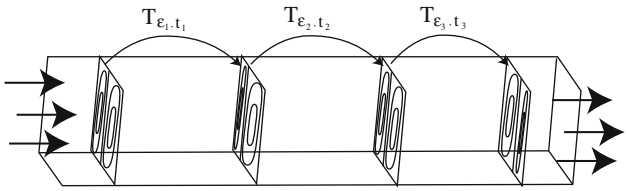

Fig. 2 Schematic of the kinematic model of the channel flow showing different cross-sectional flows along the channel and the flow maps of taking particles from one cross-section to the next

using computational fluid dynamics (CFD) techniques can also be expensive and time consuming. Both approaches require trial-and-error in order to develop geometries and methods for generating secondary flow patterns leading to optimal mixing. There is a need for a general framework and understanding of the kinematic issues required of the secondary flow structures that is *independent* of the particular manner in which the secondary flows are created, which is the subject of this article.

In Sect. 2, we develop a basic kinematic model of a cross-sectional flow having a separatrix whose location can be varied. This is the same model considered in Sturman and Wiggins (2009) and will form the basic flow structure used in our kinematic model for the channel flow. In Sect. 3, we describe the variance of concentration and our method for its computation. In Sect. 4, we describe the Eulerian indicator for quantifying the amount of streamline crossing created by the secondary flows. In Sect. 5, we use the variance of concentration to examine the predictions of the Eulerian indicator for the different flow configurations under consideration. Finally, in Sect. 6, we present our conclusions, as well as some issues for future investigations.

2 Kinematic model for the "blinking separatrix flow"

In this section, we will construct the kinematic model of a channel flow possessing a number of distinct secondary flows in the cross-section that vary along the axis of the channel. The cross-sectional flow has the structure of possessing a separatrix that divides the flow into two recirculation regions, or *gyres*. The kinematic model for the channel flow that we construct follows almost directly from the model in Sturman and Wiggins (2009), with trivial modifications. However, for completeness, in Sect. 2.1, we provide details of the derivation of the cross-sectional flow having a separatrix dividing the domain into two gyres having no-slip boundary conditions. In Sect. 2.2, we use this model of a cross-sectional flow to derive a kinematic model of a channel flow that is more general than that given in Sturman and Wiggins (2009).

Kinematic models continue to play a fundamental role in our understanding of chaotic mixing from the dynamical systems point of view, see Ottino (1989). The "blinking vortex flow" of Aref (1984) was among the earliest such kinematic models and it, and its descendants, have had a substantial influence on how we think of chaotic mixing and transport. The model we develop is similar in spirit, but it utilizes a more complex flow structure (e.g., separatrices and multiple recirculation regions) for the regions to which the flow "transitions." It is accurate to refer to it as the "blinking separatrix flow."

2.1 A kinematic model for a cross-sectional flow possessing a vertical separatrix

Following Sturman and Wiggins (2009), we first consider the "standard" streamfunction for a cellular flow, consisting of a single recirculation region defined on the unit cell, $\mathcal{S} = [-1, 1] \times [-1, 1]$, with "free-slip" boundary conditions. The streamfunction is given by $\Psi_1(x, y) = \cos(\pi x/2)\cos(\pi y/2)$. A geometrically similar flow consisting of a single recirculation region with no-slip boundary conditions on the unit cell, $\mathcal{S} = [-1, 1] \times [-1, 1]$,

can be obtained by modifying the standard cellular flow streamfunction as follows:

$$\begin{aligned}\Psi_2(x,y) &= -\cos(\cos(\pi x/2)\cos(\pi y/2)) \\ &= -\cos(\Psi_1(x,y)).\end{aligned} \tag{1}$$

The velocity field corresponding to this streamfunction is given by:

$$(\dot{x},\dot{y}) = \left(\frac{\partial\Psi_2}{\partial y}, -\frac{\partial\Psi_2}{\partial x}\right) = (u_x(x,y), u_y(x,y)) \tag{2}$$

where

$$u_x(x,y) = -\frac{\pi}{2}\cos\frac{\pi x}{2}\sin\frac{\pi y}{2}\sin\left(\cos\frac{\pi x}{2}\cos\frac{\pi y}{2}\right), \tag{3}$$

$$u_y(x,y) = \frac{\pi}{2}\sin\frac{\pi x}{2}\cos\frac{\pi y}{2}\sin\left(\cos\frac{\pi x}{2}\cos\frac{\pi y}{2}\right). \tag{4}$$

It is easy to verify that the velocity field is zero on the boundaries of $\mathcal{S}$, and has a stagnation point at $(x, y) = (0, 0)$. Using this cellular flow, we construct a flow in the rectangular domain $\mathcal{Q} = [-1, 2] \times [-1, 1]$ having the desired properties. It consists of two cellular flow patterns, divided by a separatrix consisting of a vertical streamline at $x = s$. The velocity field corresponding to the desired flow is given by:

$$\begin{aligned}(\dot{x},\dot{y}) = L(x,y) &= \left(u_x\left(\frac{x-b_1}{c_1}, y\right), \frac{1}{c_1}u_y\left(\frac{x-b_1}{c_1}, y\right)\right) \\ &(x,y) \in [-1, s] \times [-1, 1], \\ (\dot{x},\dot{y}) = R(x,y) &= \left(-u_x\left(\frac{x-b_2}{c_2}, y\right), -\frac{1}{c_2}u_y\left(\frac{x-b_2}{c_2}, y\right)\right) \\ &(x,y) \in [s, 2] \times [-1, 1],\end{aligned} \tag{5}$$

where the parameters are such that the cellular flows defined by L and R have stagnation points of centre type linearized stability at $x = b_1$, $y = 0$ and $x = b_2$, $y = 0$, respectively, in a domain of half-width c_1 and c_2, respectively. The domain being defined as $\mathcal{Q} \equiv [-1, 2] \times [-1, 1]$ requires that these parameters must satisfy $b_1 + 1 = c_1$ and $2 - b_2 = c_2$. Requiring that the cellular flows are divided by a separatrix at $x = s$ implies that $s = 2 - 2c_2$ and $s = 2c_1 - 1$. Note that particles on the streamlines defined by L move in a counter-clockwise sense while particles on the streamlines defined by R move in a clockwise sense. The separatrix $x = s$ is a line of stagnation points.

The location of the separatrix is controlled by the choice of the parameters b_i, c_i, $i = 1, 2$, but b_i and c_i are related as given above. Looking at this another way, the values of b_i and c_i depend only on the position of the separatrix, so to reflect this we introduce a single parameter ε such that $c_1 = 3/4 - \varepsilon/2$ and $c_2 = 3/4 + \varepsilon/2$. Thus, when $\varepsilon = 0$ the separatrix lies in the middle of the rectangle $\mathcal{Q}$, at $x = 0.5$. Increasing ε has the effect of moving the separatrix to the left, until it meets the boundary $x = -1$ at $\varepsilon = 1.5$, while decreasing ε from zero has the effect of moving the separatrix to the right, until it meets the wall $x = +2$ at $\varepsilon = -1.5$. Figure 1a, b illustrated two cases. To explicitly denote this dependence of the location of the separatrix on the parameter ε, we write $L(x, y) = L_\varepsilon(x, y)$ and $R(x, y) = R_\varepsilon(x, y)$.

2.2 A kinematic model for multiple secondary flows in the cross-section

The kinematic model of the secondary flow in the cross-section contains a vertical separatrix from Sect. 1, which is now used to construct our kinematic model for a channel flow. We fix $\varepsilon = \varepsilon_i$ and begin by constructing the time-t_i (for the moment, i is just an arbitrary index) map of the flow generated by (5) as follows:

$$T_{\epsilon_i,t_i} = \begin{cases} \text{Time-}t_i \text{ map under } L_{\epsilon_i}(x,y) \text{ if} & x < 0.5 + \epsilon_i \\ \text{Time-}t_i \text{ map under } R_{\epsilon_i}(x,y) \text{ if} & x \geq 0.5 + \epsilon_i \end{cases} \tag{6}$$

The sequence ε_i, $i = 1, ..., n$ defines a sequence of cross-sectional flows with corresponding times t_i, $i = 1, ..., n$, which are the times taken by a particle located at the cross-section defined by ε_i to flow to the cross-section defined by ε_{i+1} (where it then experiences the cross-sectional flow defined by ε_{i+1}). The evolution of particles down the channel after time $t_1 + \cdots + t_n$ is therefore given by the following composition of maps:

$$T \equiv T_{\epsilon_1,t_1} \circ T_{\epsilon_2,t_2} \circ \cdots \circ T_{\epsilon_n,t_n}(x,y). \tag{7}$$

In Fig. 2, we show a schematic illustration of the kinematic channel flow.

The kinematic model of the channel possesses a great deal of flexibility that enables a broad range of mixing studies. In particular, the mixer studied in Stroock et al. (2002) contained two periodically alternating flow patterns where the separatrices in the secondary flows are symmetrically located with respect to the mid-line of the channel. In the kinematic model this can be achieved by requiring the two choices of ε to satisfy $\varepsilon_1 = -\varepsilon_2$. In this case, the map defining the flow is given by $T = T_{\epsilon_1,t_1} \circ T_{\epsilon_2,t_2}(x, y)$. The evolution of particles down the channel after time $n(t_1 + t_2)$ is given by $T^n(x, y)$, which is T composed with itself n times. This particular case of the kinematic model was analyzed in Sturman and Wiggins (2009) where it was found that $t_1 = t_2 = 1$, $\varepsilon_1 \approx 0.5$, $\varepsilon_2 = -\varepsilon_1$ yielded the optimal mixing situation, which is in agreement with the results in Stroock et al. (2002).

The central question that we will consider in our development of tools for predicting optimal mixing is

whether or not more freedom in the choice of the flow structure for two secondary flows allows for "better mixing" than what has been observed in the "symmetric" two secondary flow case, and whether or not including a third *distinct* secondary flow in the channel improves mixing?

Building on the work done by Sturman and Wiggins (2009), this study expands the parameter search in order to determine the best flow configurations. The initial study done limited the values of ε_1 and ε_2 such that $\varepsilon_2 = -\varepsilon_1$, making it a one dimensional (1D) analysis where the only degree of freedom is ε_1. This study considers a two secondary flow case, where (ε_1, ε_2) vary independently of each other, making it a full two dimensional (2D) analysis. Finally, adding a third secondary flow, where all three parameters are independent (ε_1, ε_2, ε_3), was performed for a three dimensional (3D) study.

We close this section by remarking that the kinematic model is no substitute for direct numerical simulation of a mixer. However, it does faithfully reproduce the *kinematic* features of the channel type micromixers described above and allows us to perform a detailed consideration of the variation of these kinematic features in a way that is currently not possible using CFD techniques with existing computing resources. Nevertheless, there are certain features of the kinematic model that should be taken into account when considering specific applications. One is that the velocity is zero on the separatrix between the two recirculation regions (although this characteristic does not directly affect "streamline crossing"). Another feature to be aware of is that the maximum shear in one of the recirculation regions increases as its horizontal width decreases. The final feature that we wish to point out is that the "axial flow" in this kinematic model is independent of the location in the cross-section. This could be dealt with by modeling the axial flow with an applied Poiseuille flow (as is done in Stroock and McGraw (2004), Chen and Stremler (2009), Song et al. (2008), for example). However, if the flow was driven by the electro-osmotic force, rather than pressure, this would not be an issue (Pacheco (2008)). Nevertheless, we believe our results obtained from the kinematic model will provide a guide in the design of computational experiments, much as other kinematics models have done in different contexts.

3 Degree of mixing of two fluids: variance of concentration

We will require a Lagrangian diagnostic to quantify the degree of "mixedness" of fluids after a given time interval. There is significant literature on this subject; see the recent review of Funakoshi (2008). We will use the normalized variance of concentration as proposed by Danckwerts (1953a, 1953b). This has the advantage of being intuitively clear, as well as being widely used. We consider a mixture of two separate fluids, a "red" and a "green" fluid. The *concentration* of red fluid is defined as:

$$c = \frac{\#\text{red}}{(\#\text{red} + \#\text{green})}. \tag{8}$$

where #red, #green denote the number of red particles and the number of green particles, respectively. For a sample with equal parts red and green, the concentration of red over the whole domain is 50%. The initial condition considered here consists of all red particles starting in the left half and all green particles starting in the right half of the channel. As the system evolves, the two samples move together in a complicated pattern, i.e., they mix. In order to understand and quantify the mixing process, the domain is divided into smaller regions, or "bins," and, at each time, the local concentration in each bin is calculated. Mixing is quantified by computing the difference between the local concentration in each bin and the concentration over the entire domain (which does not change in time), squaring the difference, and then averaging over all the bins that comprise the domain. At a given time, the variance of the local concentration to the average over the whole domain is defined as:

$$\mathcal{V}(t) = \frac{1}{N_{\text{bins}}} \sum_{i=1}^{N_{\text{bins}}} (c_i(r_i, t) - c_{\text{avg}})^2. \tag{9}$$

The concentration calculation is performed for each bin so that local variances of the concentration capture the spatial behavior of mixing over the domain. The size of the bins is chosen so that the total number of particles tracked in each bin is always greater than 20 particles. This division of the domain, typically from 3,000 up to 10,000 bins, allows a local concentration to be computed in each bin at a given time, which we denote by $c_i(r_i, t)$, where i is the index labeling a bin and r_i denotes the position of the bin. Since the concentration of red over the entire domain does not change in time, the average concentration over the entire domain, denoted c_{avg}, is constant in time and equal to 50%.

The variance is a measure of how different each local concentration is relative to the average. For a domain with two fluid types introduced in equal amounts—half on the left, half on the right, the range of values for the variance of concentration is [0, 0.25]. For the case of a randomly mixed fluid, each bin should have a value for the concentration of red particles of 50%. The closer every bin in the sample is to 50%, the closer the value of the variance will be to *zero*, which serves as a goal value for good mixing.

The time-dependence of $\mathcal{V}(t)$ is fitted to the expression:

$$\mathcal{V}(t) = (A - \text{bias})e^{-t/\tau} + \text{bias} \tag{10}$$

where the parameter τ is the time constant for the decay of $\mathcal{V}(t)$. After simulating the decay of variance for

approximately 25,000 flows, the general behavior observed of the decay of variance of concentration is exponential. A fraction of the flows discussed, however, show an additional behavior in that the decay is delayed by a small amount of time, which is discussed in Sect. 5. To account for the range of behaviors for the full set of flows considered, the decay of variance of concentration is fitted from $6 < t_{\text{fit}} < 30$. The initial offset, $t_{\text{initial}} = 6$, avoids initial particle placement issues, which will be discussed in Sect. 5. The final time, $t_{\text{final}} = 30$ is chosen to be long enough that the onset of asymptotic behavior is observable. The parameters τ and bias in the fit provide an indication of the quality of mixing. Small values of both τ and bias lead to the best mixing situation, while having large values for either parameter leads to poor mixing.

In this study, the two and three secondary flow cases were systematically calculated along a grid of epsilon values. Epsilon values were chosen ranging from $[-1.4, +1.4]$ in steps of 0.1. For the two secondary flow case, calculations were performed on a grid of 29×29 resulting in 841 values of $(\varepsilon_1, \varepsilon_2)$. For the three secondary flow case, calculations were performed on a grid of $29 \times 29 \times 29$ resulting in 24,389 values of $(\varepsilon_1, \varepsilon_2, \varepsilon_3)$ for which the variance of concentration was calculated. Each unique set of epsilon values will be referred to as a "configuration" of the flow in the subsequent discussions.

For each flow configuration, the variance of concentration as a function of time has been calculated and the values of τ and the bias were fitted. The scatter plot of the τ–bias plane gives an idea of the values of the parameters and their quality of mixing.

In each of these cases, in order to determine good mixing from bad, the fit parameters from $\mathcal{V}(t)$ are analyzed. Figure 3a, b shows the time constant, τ, versus the bias for the two and three secondary flow cases, respectively. There are three easily identifiable regions of parameter space seen in these figures. In the upper left-hand corner, where τ is high and bias is low, are the configurations that will eventually mix well, given enough time. These are slow mixers, typically with a single, large gyre structure somewhere in the domain with smaller, satellite gyres located on the sides. In the lower right-hand corner, where the time constant is low and the bias is high, are configurations that will never mix. Typically, this is a result of significant island structures present, as seen in the Poincaré maps shown in Fig. 4a, b. These barriers to mixing lead to a significant bias term. Note that the time constant can be quite low for these poor mixers as the variance of concentration has very little to drop from the unmixed value of 0.25 down to the asymptotic values given by the bias term. This indicates that using τ, the time constant of the decay of variance of concentration alone as a diagnostic for "good mixing" can be misleading as the variance of concentration for these mixers can decay very quickly, but not very far. The lower left-hand corner (low τ, low bias) is the region of good mixers. We will examine these regions in more detail in later sections.

The figures clearly show that the characteristic time scale, τ, is not enough to determine the most complete and fastest mixers. The bias term must be considered as well. For these reasons, the "quality of mixing'' for this article is defined by the variance of concentration at end of the channel, $\mathcal{V}(t_{\text{final}} = 30)$, which accounts for both "completeness" of mixing (low bias) as well as the highest rate, or "speed," of mixing (low τ); where lower values of the variance of concentration correspond to better mixing.

An examination of Fig. 3a, b immediately leads us to one of our conclusion for this work. The best three secondary flow mixers are better than the best two secondary flow mixers in the since that the time constant is shorter for the low bias cases. An explanation will be given in the results section, Sect. 5.

The value of the variance of concentration, $\mathcal{V}(t_{\text{final}} = 30)$, at the end of a channel is used to sort the different configurations, defined by particular choices of epsilons, into four sets of mixing, labeled: "best," "good," "medium," and "poor." Table 1 shows the range of values used to determine the classification of mixers based on this scheme. The "best" mixing is achieved by the 10% of configurations with the lowest variance of concentration. The "good" mixers are the following 20% of configurations with slightly higher values than the best. "Medium" flow configurations comprise the next highest 20% of values, and the remaining 50% of the variance values are considered "poor" mixing. Note the numerical ranges for the cases in the table. The three secondary flow case outperforms the two secondary flow case significantly.

In Figs. 3, 7, and 8, the four cases of mixing are indicated by colored dots. The "best" mixing case are the largest dots, colored red. "Good" mixing are the next largest dots, colored blue. "Medium" mixing are smaller dots colored green and the smallest dots represent "poor" mixing are colored cyan. We will see that these four dots can be placed in the appropriate location in the epsilon parameter plane or cube (which we refer to as "dot plots"). Surface plots of the Eulerian indicator shown side by side with the dot plots allows us to correlate the quality of mixing with the value of the Eulerian indicator.

4 Eulerian indicator—α—transversely intersecting streamlines

In Sturman and Wiggins (2009), Eulerian indicators were introduced as a method of characterizing the kinematic features of the *velocity field* that are responsible for good

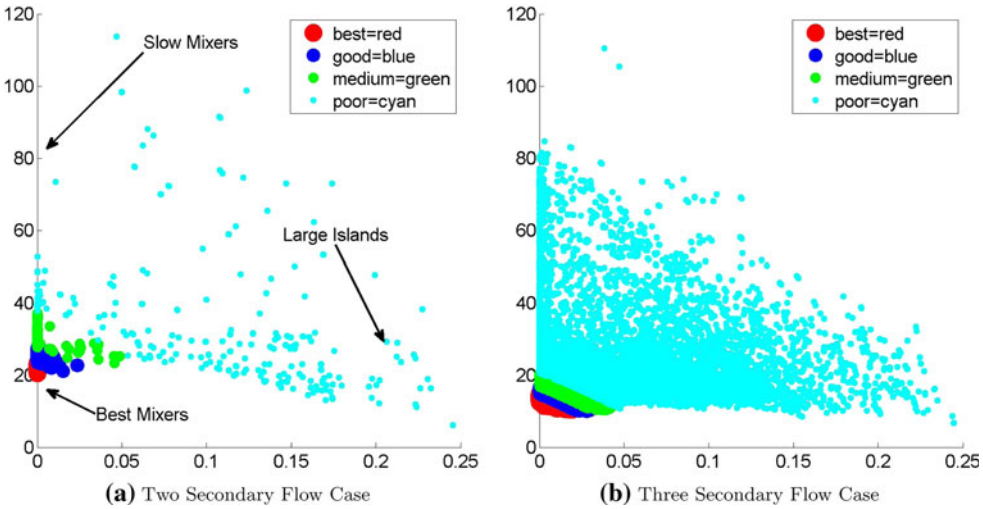

Fig. 3 Values of the time constant, τ, versus the bias from the fit of $\mathcal{V}(t)$for the case of two secondary flows, (ε_1, ε_2) and the three secondary flow case (ε_1, ε_2, ε_3)

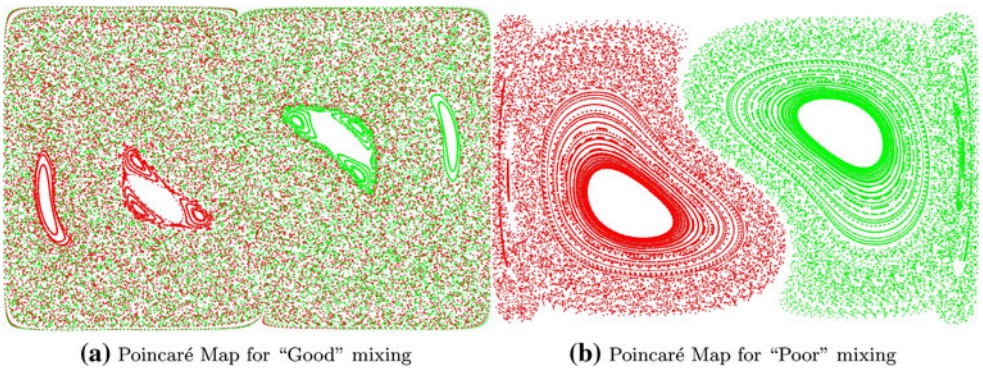

Fig. 4 Poincaré maps for two secondary, symmetric flows. **a** shows a Poincaré map for a separatrix at $\pm$ 0.8 and **b** has a separatrix at $\pm$1.2. The spatial domain shown spans the rectangle $\mathcal{Q} = [-1, 2] \times [-1, 1]$

Table 1 Table of mixing quality and thresholds with respect to the decay of variance of concentration

Type	Mixing quality	Percentage of values in range	Range of $\mathcal{V}(t_{\text{final}})$	Dot color	Qualitative description
2D	Best	10	<0.069	Red	Mixes fastest and most thoroughly
	Good	20	0.069–0.085	Blue	Mixes quickly and well
	Medium	20	0.085–0.113	Green	Mixes to some degree
	Poor	50	>0.113	Cyan	Mixes poorly and/or slowly
3D	Best	10	<0.033	Red	Mixes fastest and most thoroughly
	Good	20	0.033–0.042	Blue	Mixes quickly and well
	Medium	20	0.042–0.058	Green	Mixes to some degree
	Poor	50	>0.058	Cyan	Mixes poorly and/or slowly

mixing. In particular, Eulerian indicators for quantifying the notion of "streamline crossing" (Ottino 1990) and "transversely oriented shears" (Villermaux et al. 2008) were developed in a setting that is applicable to the kinematic model of the channel flow with two distinct secondary flows in the cross-section. It was found that the Eulerian indicator quantifying "streamline crossing" followed the decay of variance curve (the Lagrangian diagnostic) closely for the kinematic model having two distinct secondary flows in the cross-section, but where the separatrices were symmetrically related with respect to the location of the vertical mid-line of the channel. Here we generalize the Eulerian indicator quantifying "streamline crossing" to the case of n distinct secondary flows in the cross-section where the separatrices associated with each secondary flow can be arbitrarily located in each secondary flow. Moreover, we want to point out that the applicability of the Eulerian indicator is *not* limited to kinematic models. It is a general predictive tool that can be applied to a numerical determined velocity field. The analysis in this

paper is carried out for a kinematic model since it allows for an exhaustive exploration of parameter space that would not otherwise be possible.

Before defining and giving explicit formulae for the Eulerian indicator, alpha, we need to establish the setting and notation. The two dimensional secondary flows in the cross-section are given by the streamfunction ψ_{ϵ_i}, which produces equations for fluid particle trajectories $(\dot{x}, \dot{y}) = (\partial\psi_{\epsilon_i}/\partial y, -\partial\psi_{\epsilon_i}/\partial x) = (u_x^{(i)}(x,y), u_y^{(i)}(x,y)), \quad i = 1, ..., n$, where n is the number of secondary flows experienced by fluid particles as they move down the channel.

At each point (x, y) of the flow domain we can associate an angle between streamlines associated with two adjacent secondary flows as follows. The angle between tangents to these two streamline patterns, defined by the level sets of ψ_{ϵ_i} and $\psi_{\epsilon_{i+1}}$ can be easily computed, since the tangent to the streamline defined by the streamfunction ψ_{ϵ_i} through (x, y) is given by the vector $\mathbf{v}_{\epsilon_i} = (u_x^{(i)}(x,y), u_y^{(i)}(x,y))$. Then the angle between such vectors is given simply by

$$\alpha_{i,i+1}(x,y) = \cos^{-1}\frac{\mathbf{v}_{\epsilon_i}\cdot\mathbf{v}_{\epsilon_{i+1}}}{|\mathbf{v}_{\epsilon_i}||\mathbf{v}_{\epsilon_{i+1}}|}. \tag{11}$$

An important point to note is that we do not take into account the direction of flow along the streamline—we are simply interested in the transversality of the intersection. For this reason we replace $\alpha_{i,\ i+1}(x, y)$ with

$$\hat{\alpha}_{i,i+1}(x,y) = \begin{cases} \alpha_{i,i+1}(x,y) & \text{if } 0 < \alpha \le \pi/2 \\ \pi - \alpha_{i,i+1}(x,y) & \text{if } \pi/2 < \alpha \le \pi \\ \alpha_{i,i+1}(x,y) - \pi & \text{if } \pi < \alpha \le 3\pi/2 \\ 2\pi - \alpha_{i,i+1}(x,y) & \text{if } 3\pi/2 < \alpha \le 2\pi \end{cases}$$

so that $0 \le \hat{\alpha}_{i,i+1}(x,y) \le \pi/2$. See Fig. 5.

Therefore a function of the cross-sectional coordinates and the parameters (ε_i) specifying the secondary flow patterns that we take as a measure of the cumulative degree of streamline crossing in the flow is given by:

$$\hat{\alpha}(x,y;\epsilon) \equiv \sum_{i=1}^{n} \hat{\alpha}_{i,i+1}(x,y) \tag{12}$$

where we adopt the shorthand notation $\epsilon \equiv (\epsilon_1, \ldots, \epsilon_n)$, and n is cyclic $(n + 1 = 1)$. Finally, to produce a single number representing the degree of transversality associated with the n secondary flows associated with the channel flow, we average each $\hat{\alpha}_{i,i+1}(x,y)$ over the entire cross-section, denoted $\langle\hat{\alpha}_{i,i+1}(x,y)\rangle_{(x,y)}$, and add them to obtain:

$$\bar{\alpha} = \bar{\alpha}(\epsilon) \equiv \sum_{i=1}^{n} \langle\hat{\alpha}_{i,i+1}(x,y)\rangle_{(x,y)}. \tag{13}$$

5 Results: quality of mixing and the Eulerian indicator, α

In this section, we discuss the variance of concentration results and their relation to the Eulerian indicator quantifying "streamline crossing" for the kinematic model of the channel flow in the case of two distinct secondary flows in the cross-section and three distinct secondary flows in the cross-section.

5.1 Two secondary flows: $\varepsilon = (\varepsilon_1, \varepsilon_2)$

Figure 7a, b, shows the Eulerian indicator, $\bar{\alpha}(\epsilon)$ in the $\varepsilon_1 - \varepsilon_2$ parameter space as a surface and contour plot. Figure 7c, d is the "dot plots" indicating mixing quality for the best (red), good (blue), medium (green), and poor (cyan) cases, obtained from the variance of concentration, as described in Sect. 3. For comparison with previous studies, the yellow line in Fig. 7b, given by $\varepsilon_2 = -\varepsilon_1$, corresponds to parameter values of the symmetric case studied in Sturman and Wiggins (2009). The two regions bounded by the two orange lines above and below the line $\varepsilon_1 = \varepsilon_2$ shown in Fig. 7b contain the largest values of $\bar{\alpha}(\epsilon)$ and agree well with the best mixing cases according to the variance of concentration. This confirms that our Eulerian indicator quantifying streamline crossing does indeed predict the best configurations for mixing for the case of two secondary flows.

The superimposed streamline patterns yielding the largest value of $\bar{\alpha}(\epsilon)$ correspond to $(\epsilon_1, \epsilon_2) = (\pm 0.55, \mp 0.55)$, which is close to the flow configuration of Stroock et al. (2002). Figure 7c, d shows that the best mixing

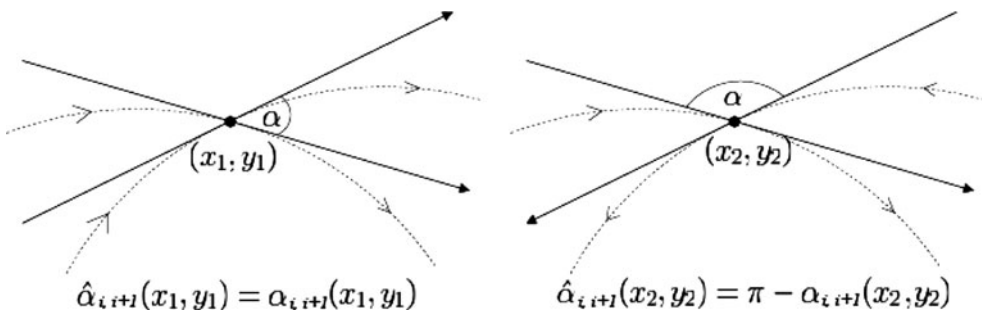

Fig. 5 Computation of $\hat{\alpha}_{i,i+1}(x,y)$.We disregard the direction of streamlines (*dotted lines*) in this computation, so that in this figure, $\hat{\alpha}_{i,i+1}(x_1,y_1) = \hat{\alpha}_{i,i+1}(x_2,y_2)$.(Figure from Sturman and Wiggins 2009)

occurs along the region of highest transversality, however, the locations corresponding to the "best mixing," as shown by the behavior of the variance of concentration, depend on the initial fluid placement, in a manner that we now explain.

When two fluids in equal amounts are initially placed in a left/right orientation, the best mixing cases are clustered around $(\varepsilon_1, \varepsilon_2) \approx (\pm 1.2, \ \pm 0.1)$. The location of the separatrix in the first secondary flow is closer to the edge of the domain, near $\varepsilon_1 = \pm 1.2$. The separatrix in the second secondary flow, near $\varepsilon_2 = \pm 0.1$, is such that it divides the large gyre in the first secondary flow. When the value of ε corresponding to the first secondary flow is close to zero the two gyres are nearly symmetric and if the two fluids are placed initially in a left/right orientation, mixing does not begin immediately. Under these circumstances, the delay in mixing causes a delay in the exponential drop of the variance of concentration. As a result of this potential delay, the fit of the variance of concentration is computed for a time window with an initial time of $t_{\text{init}} = 6$, which removes some of the effect of the initial fluids placement.

Figure 7d shows that when two fluids of equal amounts are initially placed in a top/bottom orientation, the same broad region exhibits the best mixing, within the regions bounded by the orange lines, but is shifted towards the symmetric region, studied in Stroock et al. (2002) and Sturman and Wiggins (2009). Nevertheless, for both types of initial fluid placement the regions bounded by the orange lines contain the optimal mixing cases.

The location of a separatrix in the domain and the *relative* location of separatrices in the subsequent secondary flows are the two key kinematic features that allow us to understand the behavior of the mixing process. It is important to realize that these are Eulerian features that allow us to make conclusions on Lagrangian behavior. The location of a separatrix divides the domain into two gyres, one on the left the other on the right. For separatrices located near the center of the domain, i.e., secondary flows corresponding to values of $\varepsilon \approx 0.0$, the two gyres formed are similar in size and velocity. For separatrices located near the vertical boundaries at $(x = -2, +1)$, corresponding to $\varepsilon \approx \pm 1.5$, the two gyres formed are asymmetric in size, forming a thin, fast rotating gyre and a wide, slow rotating gyre. For locations of the separatrices in between these two extremes, corresponding to $0.4 < \varepsilon < 0.9$, the gyres formed are only slightly asymmetric. Figure 1 shows streamlines in a secondary flow for $\varepsilon = -0.5$ and $\varepsilon = 0.0$. Figure 6 shows the superposition of the streamlines for two secondary flows corresponding to $(\varepsilon_1, \varepsilon_2) = (=1.2, +0.1)$ and $(-0.5, 0.5)$.

Particles at the edge of the domain, for a no-slip boundary with static walls, have velocities approaching zero. When a thin gyre is located near a wall, the higher velocities of the gyre transport particles from the edge along the streamlines at a higher rate compared to wider gyres. When the flow shifts to a new secondary flow, with a corresponding new separatrix location, those particles are then transported towards the center of the domain, participating in the mixing process. The two step process of "scraping" particles away from the edges and then transporting them towards the center with a different separatrix suggests that asymmetric flow configurations are beneficial.

To summarize, Fig. 6a, b shows the superimposed streamline patterns for the two optimal cases for the left/right and top/bottom initial placements of fluids shown in Fig. 7c, d. Figure 6a corresponds to the case where a "thin gyre" is present in one of the secondary flows and "scrapes" the edge of the domain to allow more efficient mixing by the next secondary flow pattern. Figure 6b corresponds to the case of two superimposed streamline patterns where the two separatrices are evenly spaced and divide the domain in three regions of equal area, and this is seen to maximize $\bar{\alpha}(\epsilon)$.

5.2 Three secondary flows: $\varepsilon = (\varepsilon_1, \varepsilon_2, \varepsilon_3)$

Figure 8a, c shows the epsilon parameter space for three secondary flows, where the dots represent the quality of the variance of concentration at $t_{\text{final}} = 30$ with an initial left/right fluid orientation. Figure 8b, d shows the same parameter space dot plot for values of transversality, $\bar{\alpha}(\epsilon)$. As in the case for two secondary flows, the Eulerian indicator $\bar{\alpha}(\epsilon)$ correlates well with the variance of concentration through most of the parameter space confirming that it is a predictor of mixing performance.

The three separatrix locations are obtained from the values of $\varepsilon = (\varepsilon_1, \varepsilon_2, \varepsilon_3)$. The two secondary flow case is embedded within the three secondary flow case whenever two of the three epsilon values are similar ($\varepsilon_i \approx \varepsilon_j$). When two epsilon values are close, the three secondary flow case exhibits the same behaviors of mixing described in Sect. 5.1. There are six possible ways that three epsilon values can resemble the two secondary flow case, which leads to the hexagonal structure clearly seen in Fig. 8. The six ellipsoidal regions seen in the dot plots of transversality, $\bar{\alpha}(\epsilon)$, are the 3D equivalent to the two orange regions shown in Fig. 7b. The variance of concentration at $t_{\text{final}} = 30$ shows a similar hexagonal structure to transversality, which is yet a further confirmation that $\bar{\alpha}(\epsilon)$ is a predictor of mixing performance.

Figure 9 shows cross-sectional views of contours of $\bar{\alpha}(\epsilon)$, for $[\varepsilon_1, \varepsilon_2]$ at fixed values of ε_3, with "dots" indicating the quality of mixing overlayed on each cross-section. In these figures, we show only 11 cross-sections of the 29 planes which make-up the $29 \times 29 \times 29$ cube of results. Starting at the lowest plane, Fig. 9a, ($\varepsilon_3 = -1.5$), the cross-section

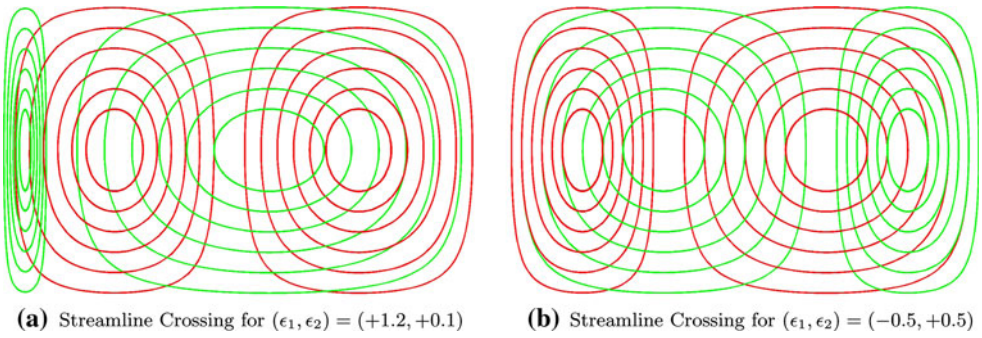

(a) Streamline Crossing for $(\epsilon_1, \epsilon_2) = (+1.2, +0.1)$ **(b)** Streamline Crossing for $(\epsilon_1, \epsilon_2) = (-0.5, +0.5)$

Fig. 6 Superimposed streamlines for two cases illustrating how transversality of the two intersecting patterns of streamlines changes over the spatial domain shown which spans the rectangle $\mathcal{Q} = [-1, 2] \times [-1, 1]$

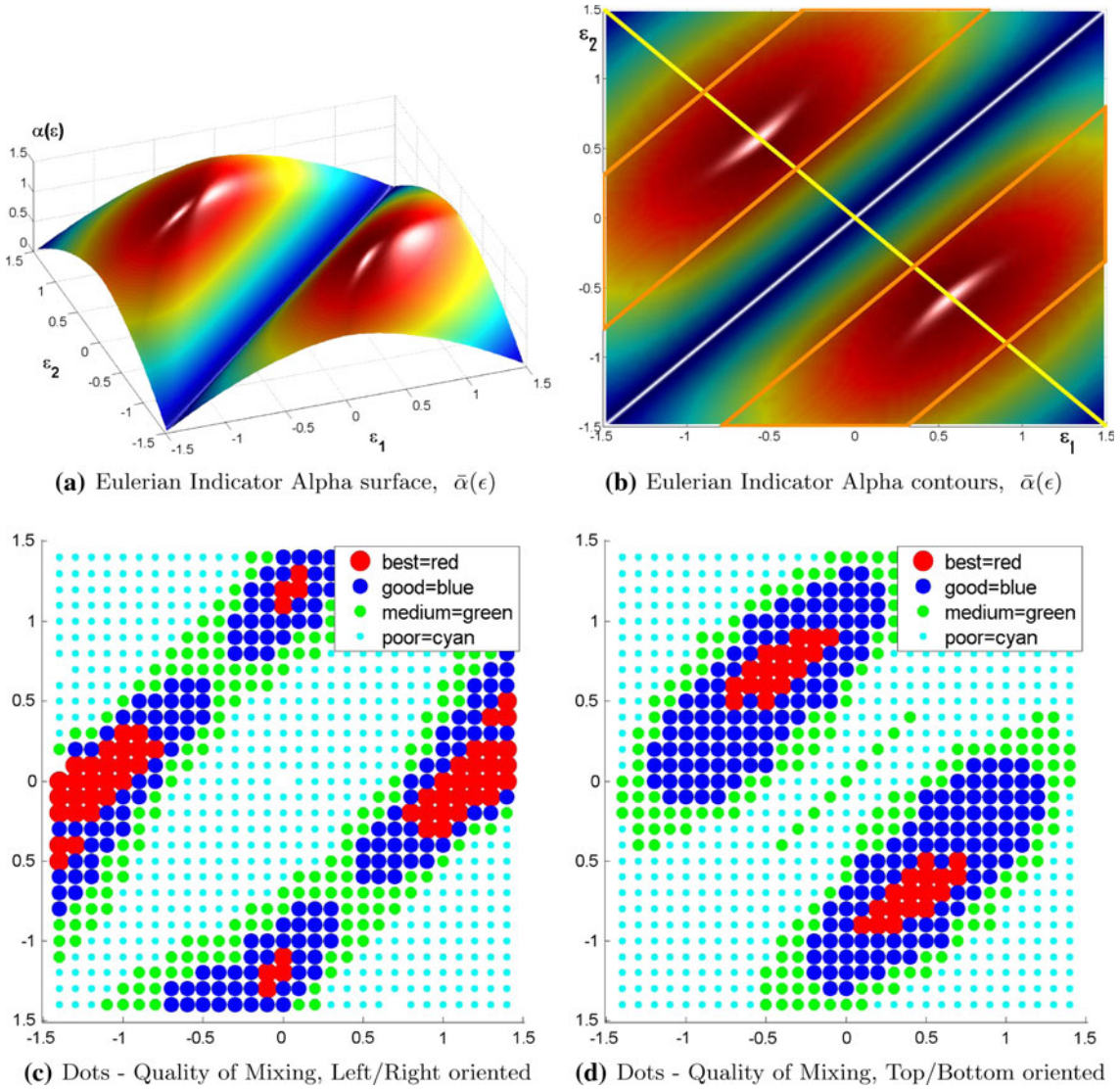

(a) Eulerian Indicator Alpha surface, $\bar{\alpha}(\epsilon)$ **(b)** Eulerian Indicator Alpha contours, $\bar{\alpha}(\epsilon)$

(c) Dots - Quality of Mixing, Left/Right oriented **(d)** Dots - Quality of Mixing, Top/Bottom oriented

Fig. 7 **a**, **b** shows the Eulerian indicator alpha across the $\varepsilon_1 - \varepsilon_2$ parameter space. **c**, **d** shows the "quality of mixing" dot plot over the same parameter space for two fluids initially placed in a left/right and top/bottom orientation, respectively. The yellow line indicates the 1D study of Sturman and Wiggins (2009)

of contours of transversality, $\alpha(\varepsilon_3 = -1.5)$, is identical to the contours of $\bar{\alpha}(\epsilon)$ in the $\varepsilon_1 - \varepsilon_2$ parameter space for the case of two arbitrary secondary flows, see Fig. 7b. This makes sense as the value of $\varepsilon_3 = -1.5$ corresponds to a separatrix located at $x = +2.0$, the far right vertical boundary, effectively making the third secondary flow one large gyre spanning the whole domain and an infinitely thin gyre located at $x = +2.0$. The other two ε values then act as

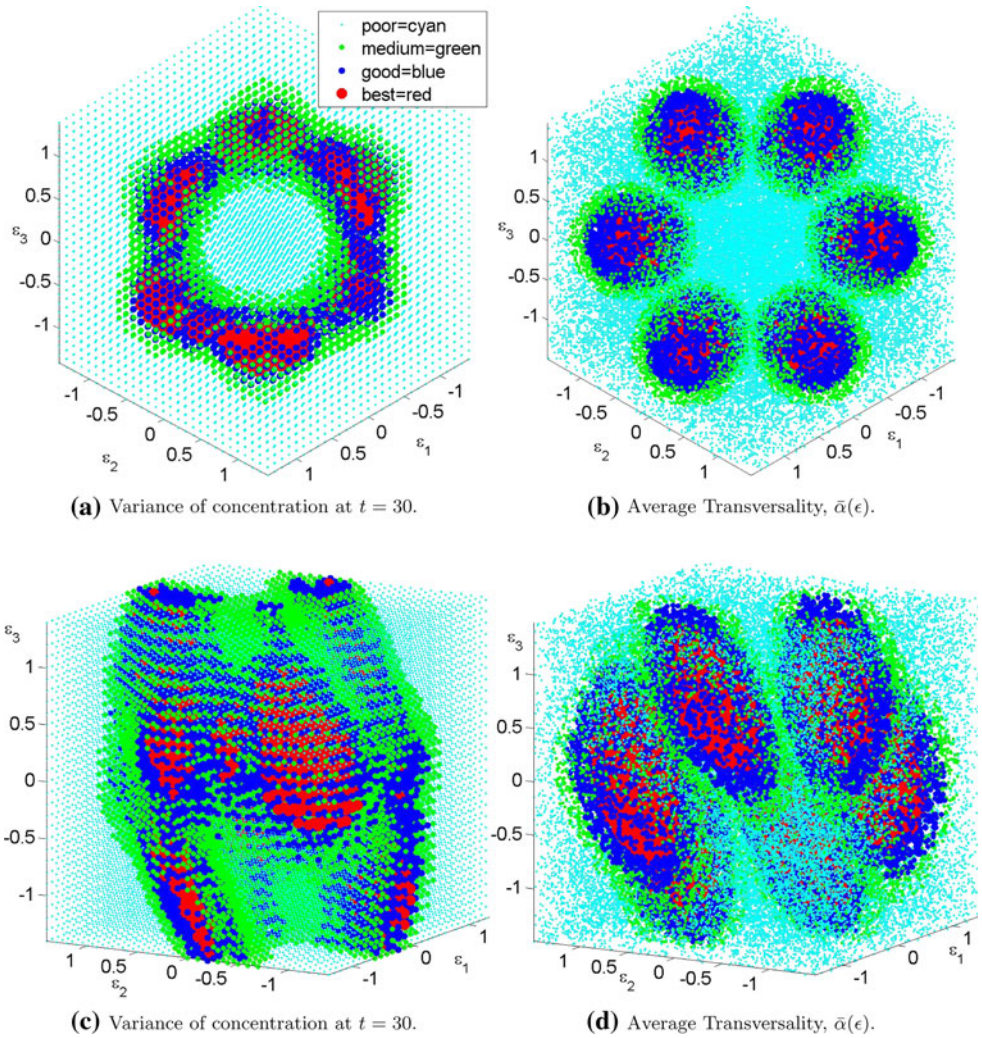

Fig. 8 Three secondary flow case (3D) spanning the epsilon space $[\varepsilon_1, \varepsilon_2, \varepsilon_3]$. **a**, **c** show the "quality of mixing" dot plot, which is the variance of concentration, $\mathcal{V}(t_{\text{final}} = 30)$. **b**, **d** shows the Eulerian indicator, $\bar{\alpha}(\epsilon)$, in a dot plot representation. The initial placement of red/green particles are left/right oriented, respectively. The viewing angle for (**a**) and (**b**) is $(\theta, \phi) = (55°, 45°)$ and for (**c**) and (**d**) is $(\theta, \phi) = (78°, 210°)$

a two secondary flow mixer followed by one large gyre. As the value of ε_3 increases from its minimum value (-1.5) up to its maximum ($+1.5$), the third secondary flow contributes two gyres to the mixing whose separatrix line moves from $x = +2.0$ down to $x = -1.0$. The third secondary flow contributes additional flow structure through one more set of streamlines to the calculation of the average transversality, as described in Sect. 4. The effect on the $\varepsilon_1 - \varepsilon_2$ parameter space can be seen in Fig. 9a–k.

Another kinematic feature from Sect. 5.1 applies in the three secondary flow case. Recall that the *two* secondary flow configurations resulting in the best mixing had one of the secondary flows containing a thin gyre, whose separatrix was located near the edge of the domain, with the other secondary flow configuration containing a separatrix located near the center of the domain. The superposition of the streamlines for those two secondary flows gave a large value of $\bar{\alpha}(\epsilon)$. As we described, the presence of the thin gyre in the secondary flow assists with transport from the boundary to the center of the domain. The opposite side of the domain, however, would *not* experience the same transport effect since the subsequent secondary flow has a separatrix near the center, see Fig. 6a. In other words, although this configuration of two secondary flows leads to decent streamline crossing and good transport, the effect of the thin gyre only affects one side of the domain. However, for the *three* secondary flow case, locations of separatrices can be chosen such that two thin gyres are placed on both ends of the domain followed by a third separatrix near the center. This three secondary flow configuration gives a large value of $\bar{\alpha}(\epsilon)$ as well provides greater transport of particles into the center from both boundaries. This is a kinematic explanation of why a three secondary flow configuration will mix better than a two secondary flow configuration, according to the behavior of the variance of concentration.

We also note that by choosing the location of the separatrices so that when the streamline patterns are superimposed, the separatrices divide the domain into regions of equal area corresponding to flow configurations which have

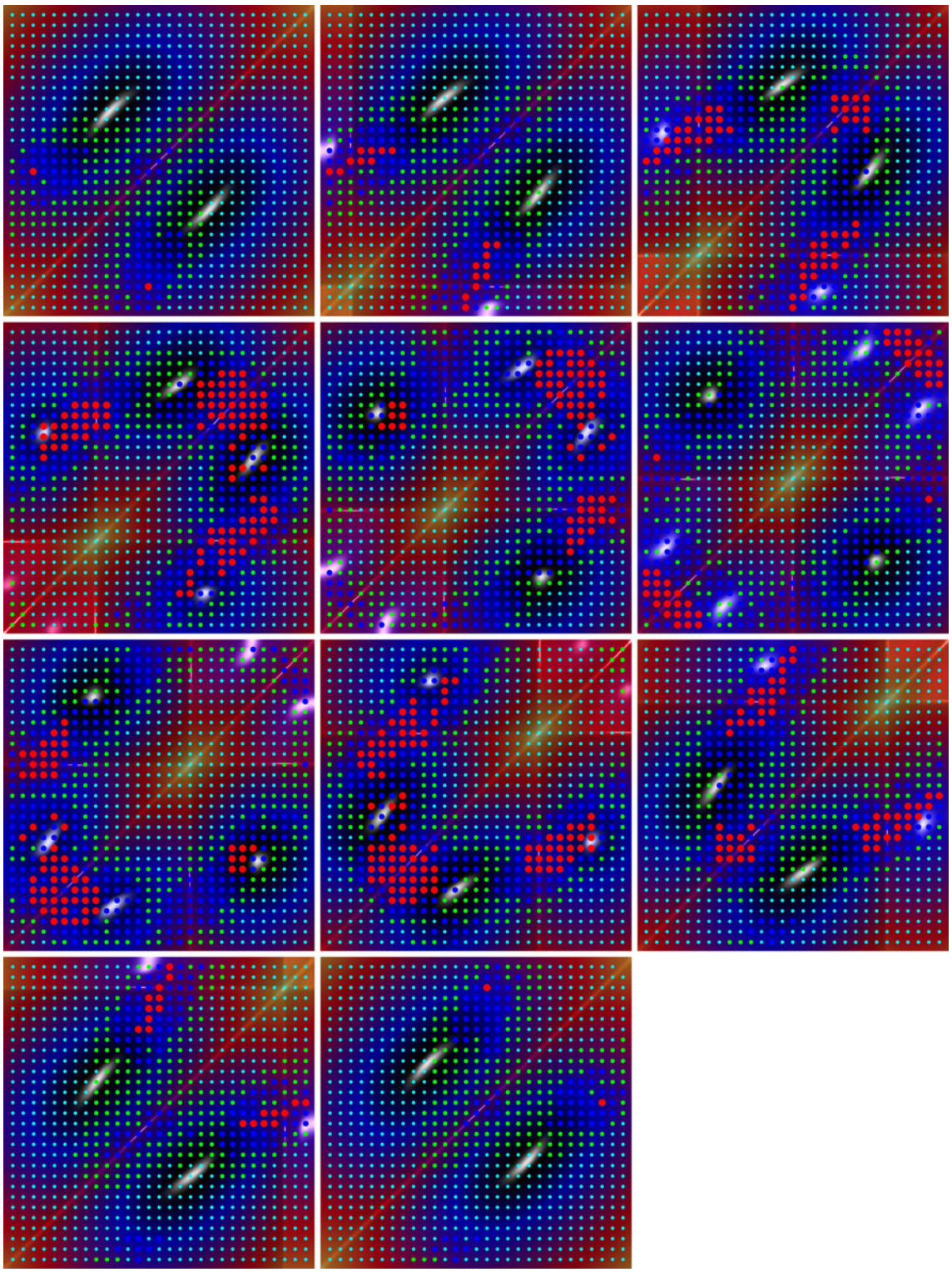

Fig. 9 Contours of the Eulerian indicator, $\bar{\alpha}(\epsilon)$, for three secondary flows. Shown here are the cross-sectional views for $[\varepsilon_1, \varepsilon_2]$ at fixed values of $\varepsilon_3 = [-1.5, -1.2, -0.9, -0.6, -0.3, 0.0, +0.3, +0.6, +0.9, +1.2, +1.5]$ shown from left to right then top to bottom, respectively. On each cross-sectional view "dots" indicating the quality of mixing are overlayed. To provide better contrast, $\bar{\alpha}(\epsilon)$ ranges from low values (*red*) to higher values (*black*)

the highest values of $\bar{\alpha}(\epsilon)$. For the *two* secondary flow case this is achieved for $\varepsilon = [-0.50, +0.50]$ and for the *three* secondary flow case it is achieved for $\varepsilon = [-0.75, 0.00, +0.75]$.

Summarizing, the regions of mixing observed in the three secondary flow case fall into a few broad categories.

- Double valued triplets, such as $(\varepsilon_2 = \varepsilon_1)$, which act similarly to the two dimensional case, creating a facet by extruding a diagonal line in the $\varepsilon_1 - \varepsilon_3$ space along a diagonal line in the $\varepsilon_1 - \varepsilon_2$ space.
- Scraping triplets—any set of ε values where two of the three epsilon values correspond to separatrices near both vertical edges of the domain with a third separatrix in the middle.
- Evenly spaced separatrix locations, which divide the domain into equal parts, giving the highest average transversality, $\bar{\alpha}(\epsilon)$.

As discussed in Sect. 3, three secondary flow configurations show faster mixing than their two secondary flow counterparts (cf. Fig. 3a, b). This improvement can be partly attributed to the fact that having three different epsilon values will inevitably bring more particles from the edges of the domain into the center, where they can mix more with the rest, and an additional contributing factor is that more streamlines leads to more regions of higher transversality.

6 Conclusions and outlook

In this article, we have generalized the Eulerian indicator quantifying "streamline crossing" developed in Sturman and Wiggins (2009) to allow for the case of more than two distinct secondary flows and applied it to a kinematic model for a steady, three-dimensional channel flow that allows for an arbitrary number of distinct secondary flows in the cross-section. The kinematic model allows for a detailed study of different flow configurations for channel type micromixers that exhibit two and three distinct secondary flows, but the Eulerian indicator does *not* require a kinematic model for its applicability.

For the case of two distinct secondary flows, we show that by appropriate choice of non-symmetrically related secondary flows the quality of mixing can be improved with respect to the case of two symmetrically related secondary flows studied earlier (Sturman and Wiggins 2009). An explanation of this improvement in terms of the geometry of the Eulerian flow structure is given. We then consider the case of three arbitrary secondary flows. The Eulerian indicator predicts the secondary flow configurations leading to the best mixing, and we showed that the three secondary flow case mixes better that the two secondary flow case. An explanation for the improved mixing is provided in terms of the geometry of the Eulerian flow structures.

A significant point here is that our result is *independent* of the way in which the secondary flows are created, e.g., patterning on the walls of the channel or electro-osmotic driving. Therefore they should prove useful in the design and optimization process for channel type micromixers in that they show ahead of time the flow structure that needs to be achieved, regardless of the manner in which the secondary flow is created.

Our results raise many issues requiring further work. We have limited our study to the case of channel type micromixers that exhibit three distinct secondary flows. We have shown that three distinct secondary flows improves mixing with respect to the situation of two distinct secondary flows. An obvious question remains concerning the understanding of the effect of more than three distinct secondary flows, as well as the axial flow rate, on mixing.

Finally, our Eulerian indicators provide a type of "metric" that can be used to assess the quality of mixing. The Lagrangian diagnostics fill a similar role, but with different requirements for their implementation. It would be useful to merge this dynamical systems approach to the assessment of mixing with computational fluid dynamics techniques for the construction of the types of flows used in micromixing. We are currently working on merging the software that we have developed in the course of this work with the NRL toolbox described in Mott et al. (2006).

Acknowledgments We have benefited very much from conversations with Elaine Oran and David Mott of the Naval Research Laboratory and Greg Voth from Wesleyan University. This research was supported by ONR grant no. N00014-01-1-0769 and No. N00014-09-WR-2-0256. SW would like to acknowledge the stimulating environment of the NSF sponsored Institute for Mathematics and its Applications (IMA) at the University of Minnesota, where this work was begun. KLM would like to thank Jeremy Bruch and Reza Malek-Madani for so many useful conversations.

References

Aref H (1984) Stirring by chaotic advection. J Fluid Mech 143:1–21

Aubin J, Fletcher DF, Xuereb C (2005) Design of micromixers using CFD modelling. Chem Eng Sci 60(8–9):2503–2516

Chen J, Stremler MA (2009) Topological chaos and mixing in a three-dimensional channel flow. Phys Fluids 21:021701

Danckwerts PV (1953a) The definition and measurement of some characteristics of mixtures. Appl Sci Res A3:279–296

Danckwerts PV (1953b) Theory of mixtures and mixing. Research 6:355–361

Funakoshi M (2008) Chaotic mixing and mixing efficiency in a short time. Fluid Dyn Res 40:1–33

Knight J (2002) Microfluidics: Honey, I shrunk the lab. Nature 418:474–475

Mott DR, Howell PB, Golden JP, Kaplan CR, Ligler FS, Oran ES (2006) Toolbox for the design of optimized microfluidic components. Lab Chip 6:540–549

Ottino JM (1989) The kinematics of mixing: stretching, chaos, and transport. Cambridge University Press, Cambridge, England. Reprinted 2004

Ottino JM (1990) Mixing, chaotic advection, and turbulence. Ann Revs Fluid Mech 22:207–254

Pacheco JR (2008) Mixing enhancement in electro-osmotic flows via modulation of electric fields. Phys Fluids 20:093603

Song H, Yin X-Z, Bennett DJ (2008) Optimization analysis of the staggered herringbone micromixer based on the slip-driven method. Chem Eng Res Des 86:883–891

Stroock AD, McGraw GJ (2004) Investigation of the staggered herringbone mixer with a simple analytical model. Philos Trans R Soc Lond Ser A 362(1818):971–986

Stroock AD, Dertinger SKW, Ajdari A, Mezic I, Stone HA, Whitesides GM (2002) Chaotic mixer for microchannels. Science 295:647–651

Sturman R, Wiggins S (2009) Eulerian indicators for predicting and optimizing mixing quality. New J Phys 11:075031

Villermaux E, Stroock AD, Stone HA (2008) Bridging kinematics and concentration content in a chaotic micromixer. Phys Rev E 77:015301(R)

Yang J-T, Huang K-J, Lin Y-C (2005) Geometric effects on fluid mixing in passive grooved micromixers. Lab Chip 5(10): 1140–1147